RSC Advances

PAPER

View Article Online
View Journal | View Issue

Cite this: *RSC Adv.*, 2023, **13**, 8299

Free-standing TiO_2 nanograssy tubular hybrid membrane for polysulfide trapping in Li–S battery†

Suriyakumar Dasarathan,‡[ab] Junghwan Sung,‡[ab] Jeong-Won Hong,[a] Yung-Soo Jo,[a] Byung Gon Kim,[ab] You-Jin Lee,[a] Hae-Young Choi,[a] Jun-Woo Park‡[ab] and Doohun Kim ‡*[ab]

During the growth of anodic TiO_2 nanotubes with a high layer thickness of greater than 20 μm, "nanograss" structures are typically formed on the outermost surface. This happens due to the fact that the engraving of the oxide tubes arises during prolonged exposure to an F- ion containing electrolyte. These TiO_2 nanotubular layers have a high aspect ratio with astonishing bundles of nanograss structures on the tube top and especially a high surface area with anatase crystallites in the tubes. By two-step anodization in synergy with the hybridization of a rubber polymer binder, freestanding nanotubular layers consisting of nanograssy surfaces with nano-crystalline particles in the tubes were successfully obtained. Under the highly efficient polysulfide trapping and electrolyte perturbation, this nanotubular hybrid membrane could deliver an enriched performance with a capacity of 618 mA h g^{-1} after 100 cycles at 0.1C in Li–S batteries.

Received 17th January 2023
Accepted 23rd February 2023

DOI: 10.1039/d3ra00349c

rsc.li/rsc-advances

Introduction

Urging for enormous power sources is ascribed to meeting the incessant flow demand in electric mobility and energy storage systems.[1–5] Present Li-ion battery-based intercalation compounds (*e.g.*, $LiCoO_2$ and $LiFePO_4$) have a limited specific energy.[6–8] Li–S batteries with a striking high energy density of 2567 W h kg^{-1} and a high specific capacity of 1672 mA h g^{-1} have generated a potential interest for such applications.[1,9–11] From the aspects of low cost, eco-friendly, and abundance, Li–S batteries depict a prominent interest in large-scale applications in the field of renewable energy.[2,12] However, two main challenges impede the commercialization of sulfur as the cathode in Li–S cells. Firstly, the specific discharge capacity of Li–S cells is limited by poor active material utilization caused by the insulating nature of dissolving polysulfides in the electrolyte. Next, the cycle life and low coulombic efficiency are affected by the combination of polysulfide diffusion and its "shuttle effect" during the redox process. The highly soluble long-chain polysulfides (Li_2S_x, $4 < x \leq 8$) are easily permeable through the separator and induces the loss of active material and severe fading of capacity. The diffused polysulfides further react with the Li anode and corrode it, which results in cell failure.[6,9,13,14]

To resolve these problems, contemporary efforts are focused on the development of new constraints for polysulfide dissolution.[12,14–18] Thus far, many approaches have been developed in physically confined polysulfides trapping in mesocarbon materials,[19–21] graphene,[22–24] and hollow carbon spheres.[20,26] However, the polysulfides diffuse out of the hydrophobic pores of carbon materials due to the fact that it does not bind to the polar and ionic sulfides because carbon is non-polar in nature.[8] Recently, Cui Yi group has shown that sulfur TiO_2 composite achieves a high specific capacity[27] and in a further study they demonstrated that the strong chemical bonds between $Ti_{(n)}O_{2(n-1)}$ and S-species contribute importantly to the improvement of the electrochemical properties.[28] Therefore, it is a remarkable approach to absorb the polysulfides into hydrophilic metal oxides such as carbon-modified TiO_2 as a separator host material. Moreover, there are also reports addressing the use of anodic TiO_2 nanotube layers in conventional Li-ion batteries.[25,29–35,40,41] These applications are commonly based on the use of TiO_2 nanotubular structures along with a titanium metal substrate as an electrode. Until now, there is ambiguity on the direct application of such free-standing membrane[38] in Li-ion batteries.

Herein, we report a novel TiO_2 nanotubular hybrid membrane preparation and application as a polysulfide scavenger in Li–S battery. Recently, Schmuki *et al.* successfully showed the preparation of pure anatase membranes for a flow-through photocatalytic application by multi-step anodization.[39] We introduced a synthetic strategy of two-step anodization

[a]*Next Generation Battery Research Center, Electrical Materials Research Division, Korea Electrotechnology Research Institute (KERI), Jeongiui-gil 12, Seongsan-gu, Changwon, Gyeongsangnam-do 51543, Republic of Korea. E-mail: kdh0121@keri.re.kr*

[b]*Department of Electro-functional Materials Engineering, University of Science and Technology (UST), Jeongiui-gil 12, Seongsan-gu, Changwon, Gyeongsangnam-do 51543, Republic of Korea*

† Electronic supplementary information (ESI) available. See DOI: https://doi.org/10.1039/d3ra00349c

‡ S. Dasarathan, J. Sung, J.-W. Park and D. Kim contributed equally to this work.

combined with polymer hybridization to prepare the free-standing TiO_2 nanoporous structure. These TiO_2 membranes have a spectacular morphology of extremely high aspect ratio nanotube layer with coalescing fiber-like porous "nanograss" on the tube top.[36] The individual tubes also have a nanoporous morphology of a highly ordered 1D structure with a TiO_2 nanoparticulated inner shell and pure TiO_2 outer wall of the nanotube.[38] Such highly ordered TiO_2 nanostructures with high aspect ratios have a fast electron/ion transport property in electrochemical applications.[44,45] In the present work, for the first time we report a novel TiO_2 nanotubular hybrid membrane preparation and its application as a polysulfide scavenger in Li–S battery. With the superior physical properties of a highly porous membrane, large amounts of polysulfides are trapped in the TiO_2 nanostructured membrane enhancing the Li-ion transport.

Results and discussion

Preparation of free-standing nanograssy tubular hybrid membrane

TiO_2 nanotube membranes were prepared by a novel approach of two-step anodization combined with polymer hybridization as shown in the schematic illustration of Fig. 1a. In the first step, nanotubular layers are formed on the Ti substrate by electrochemical anodization in fluoride ions containing the electrolyte. These anodic TiO_2 nanotube arrays are grown perpendicular to the titanium substrate with highly complied adherence. The highly porous TiO_2 nanograssy structures are typically formed on the tube tops due to the deformation of the tube walls by chemical engravings.[36] To detach the anodized TiO_2 nanograssy layers from the substrate, the layers have to be durable in the chemical etchant. In fact, even if the layer thickness is higher in order of 25 μm, the amorphous oxides are considerably dissolved out in the etchant. For withstanding the chemical etching, the entire amorphous layers (as prepared) were annealed up to 450 °C to convert them into crystalline layers. Subsequently, on the surface of the crystalline structure, a thin polymer layer of the elastic rubber binder (styrene butadiene rubber, SBR) was spin-coated for electrical insulation and especially for membrane protection without any cracking and crumbling. In the later stage of the second anodization, the tube stack was formed with other amorphous nanotubes underneath the crystalline layers, as shown in Fig. 1b.

It is noteworthy that the continued tube growth indicated that the electrolyte was able to flow locationally through the membrane without any blocking of the ion diffusion for the anodization. In the tube stack, the second layer was the amorphous sacrificial layer for the next etching step. After soaking in the H_2O_2 etchant, the amorphous layer was selectively dissolved between the substrate and the crystalline nanotube layers. The crystalline layer was detached from the substrate and floated on the H_2O_2 solution instantly after the chemical etching. Through this process, the free-standing TiO_2 nanograssy tubular hybrid membrane was obtained and directly applicated to the Li–S battery as a membrane.

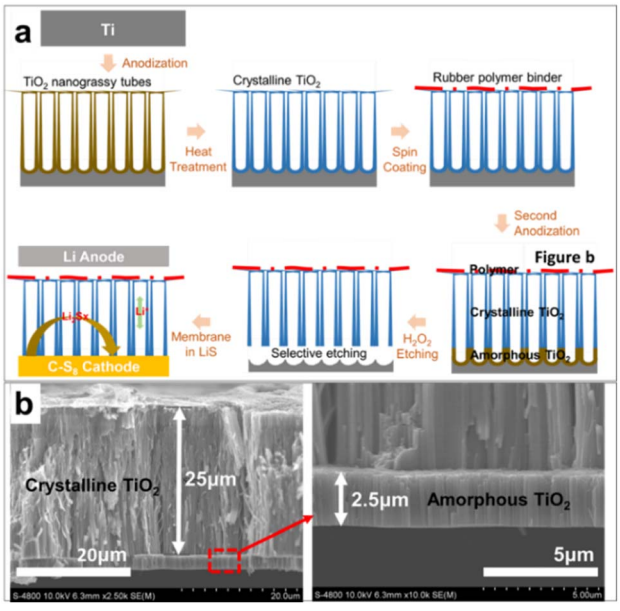

Fig. 1 (a) Schematic illustration of the fabrication of the free-standing TiO_2 nanograssy membrane and its application in Li–S battery (b) FE-SEM cross-sectional image of multi-layered TiO_2 nanotube (TNT) prepared by 2-step anodization. The magnified image of (b) showing that amorphous TNTs grown underneath the crystallized TNTs.

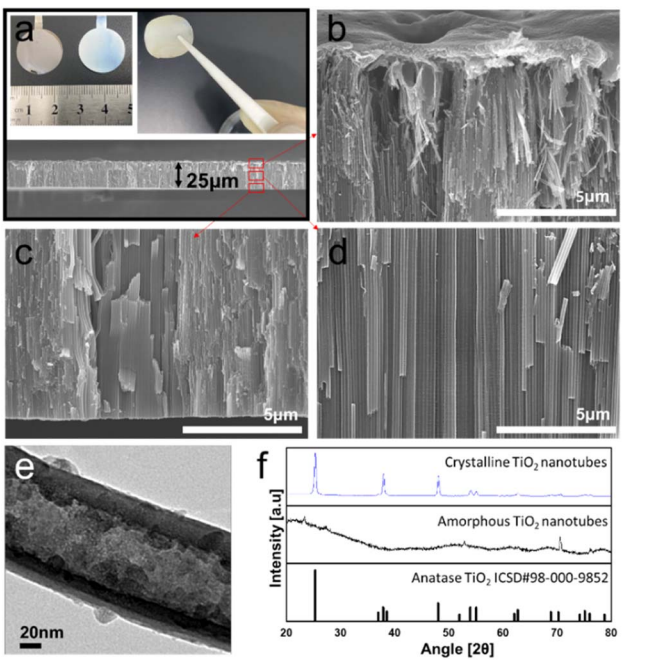

Fig. 2 FE-SEM cross-section images of (a) full view, (b) top, (c) bottom, and (d) middle view of nanograssy hybrid membrane. (e) HR-TEM image of the inner shell (IST) and outer shell (OST) of the TiO_2 nanotube membrane. (f) XRD patterns of crystalline and amorphous nanotube layers. The sharp peaks in the amorphous phase were detected from the edge part of the Ti metal substrate. Digital image of (a) represents after anodization of Ti foil (left: "as prepared", amorphous TNT) and after annealing of the anodized sample (right: crystalline TNT) with tweezer handling of the free-standing TiO_2 hybrid membrane that was prepared as described in Fig. 1.

The morphology of the free-standing nanotubular hybrid membrane is shown in Fig. 2a. The digital image shows amorphous (as prepared), annealed, and detached layers, respectively. The obtained free-standing membrane has a uniform thickness of approximately 25 μm. The cross-sectional FE-SEM images in Fig. 2b–d show the top, low, and middle parts of the TiO_2 nanotube membrane, respectively. The tube walls are well separated into individual entities with a diameter of approximately 140–180 nm. It is apparent from the top of the tube shown in Fig. 2b that the membrane surface has a very irregular morphology and the tube top walls also have disintegrated morphology that is partially etched with the initial tube layer after anodization in the NH_4F + ethylene glycol-based electrolyte.[36] The chemical etching of the TiO_2 tube wall gives rise to the falling down of tube walls with the formation of the TiO_2 nanoporous grassy structure (TNT) (see Fig. S1 in the ESI†). On the tube top, an approximately 1 μm thick polymer binder covers the entire surface regularly. As shown in the image from the top to bottom part, the TiO_2 nanotubular membrane has an extremely high aspect ratio with both sides open, *i.e.*, flow-through membrane.[37] This highly ordered TiO_2 structure covering the porous tube top has a spectacular characteristic for absorbing the chemical products in the framework as a membrane. Moreover, individual tubes also consist of a highly porous structure as shown in the TEM image of Fig. 2e. TiO_2 nanocrystallites in the range of several nanometers are present in the outer tube wall and the carbon species are mainly incorporated in the inner shell during the heat treatment process with the remaining ethylene glycol-based electrolyte,[38] which is favorable in a view of chemical absorption and ionic pathways in the nanostructure. The XRD pattern of this sample shown in Fig. 2f confirmed the conversion to a crystalline anatase structure due to the annealing temperature of 450 °C.

Nano grass formation and polymer hybridization

We investigated the anodization time dependence for the nanograss formation (see Fig. S1 in the ESI†). In the anodization of the Ti substrate in the NH_4F + ethylene glycol-based electrolyte, the chemical etching occurred on the earliest formed tubes. This process accelerated substantial thinning and finally disintegrated parts of the tube walls, which led to nanograssy appearance on the tube tops.[36] Anodic TiO_2 nanotubes are vertically split off by electric-field-directed chemical etching and fall down as a bundled TiO_2 nanoporous structure typically known as the "nanograss" structure is formed on the top layer. As shown in Fig. 3a and b, it is apparent that on the top surface, TiO_2 nanograssy bundles are formed with an extremely high aspect ratio. Coalescing TiO_2 fibers have highly nanoporous networks, which also have similar morphology to that of the commercial organic separator but they are nanoscaled. Therefore, such nanoporous reservoirs can be available for use as polysulfides inhibitor with 3-dimensional accessible pathways for Li-ion diffusion. Even after polymer coating on the nanograssy structures, the membrane was not blocked, as shown in Fig. 3c and d. The polymer styrene butadiene rubber (SBR) binder is uniformly coated on the nanograss but the macropores are still present on the surface that shows the

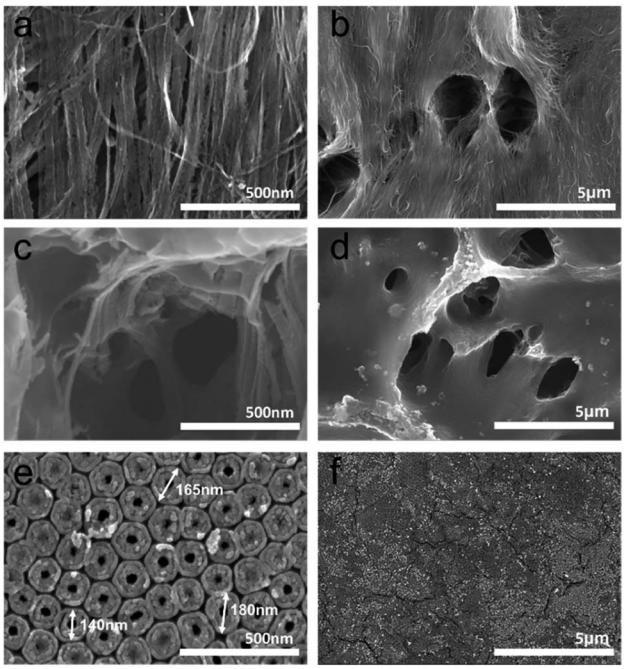

Fig. 3 FE-SEM image of nanograss surface view in high and low magnification before (a and b), after (c and d) polymer coating, and (e and f) double-walled nanotubes at the bottom surface.

membrane structure (see Fig. S2 in the ESI†). Meanwhile, from scanning electron microscopy of the bottom surface view in Fig. 2e and f, it is evident that the TiO_2 nanotube wall consists of two different regions: an outer shell of the tube (OST) and the inner shell of the tube (IST) that are typically formed during the heat treatment at 450 °C. The total thickness of these two parts changes along the tube wall (see Fig. S1 in the ESI†). The thickness of OST and IST increase along the tube wall a few nm from the tube top to bottom of approximately 25 nm and 35 nm, respectively.[38] However, the nanoscopic sizes of the TiO_2 nanotubes strongly depend on the anodizing parameters such as the electrolyte species and applied voltage.[42] After anodization, the electrolyte species that are present in the IST, especially carbon-based compounds from the inner shell evaporate after the annealing procedure resulting in the inner shell becoming porous in nature that can be revealed from the TEM image shown in Fig. 2e and the FE-SEM image in Fig. 3e. The distribution of carbon in the tubes is well co-ordinated in IST and the further annealing process results in the porous structure of double-walled open tubes (DWOT), *i.e.*, the OST becoming compact and the IST becoming porous with a carbon-rich layer.[38] TiO_2 nanocrystallites in the OST are formed along the carbonized inner wall of DWOT. The nanoporous architecture of double-walled open tubes with the nano grassy structures has a unique morphology to be used in the highly-efficient polysulfide absorbing membrane.

Electrochemical analysis

In Li–S battery, a series of electrochemical reaction converted the long-range polysulfides of S_8 into lower-order polysulfides of Li_2S that is almost insoluble and precipitate from the organic electrolyte at the transition point between the upper and lower

plateau profiles (see Fig. S3 in the ESI†). Thus, the shuttle effect induces the formation of Li_2S insulating layers on the surface of the Li-metal anode and deteriorates its electrochemical performance owing to the degradation of the active material, capacity fading, cycling stability deterioration, and a decrease in ionic conductivity. The passivated layer formed on the anode side is a critical factor in increasing the resistance and accelerating Li metal anode oxidation, thus reducing the cycle stability of Li–S batteries.[27] Fig. 4a shows the cyclic voltammetry plots (CV) of the nanotubular membrane for the initial five cycles with a scan rate of 0.1 mV s^{-1} in the voltage range of 1.5–3.0 V. The cell was initially swept from the open-circuit voltage to 3.0 V, ensuring a complete conversion of Li_2S_6 to S_8/Li_2S_8 transformation. After the active material encapsulation *via* the *in situ* conversion of dissolved polysulfides, the CV curves show the typical two-step sulfur reduction process. The cathodic peaks at 2.29 V and 1.98 V represent the transition from elemental sulfur to long-chain polysulfides (Li_2Sn, $4 < n < 8$). The two peaks are related to the transition from long-chain to short-chain polysulfides (Li_2S_2 to Li_2S), respectively.[6,9] The subsequent anodic cycle (3–5th cycles) of the oxidation peaks shifting to the position at 2.5 V is related to the complete conversion of Li_2S into elemental S during the formation of Li_2S_n ($n > 2$).[11] The two Peaks located at 1.72 V(III) and 2.03 V(IV) clearly reveal the lithiation and delithiation of the TiO_2 nanotubular membrane.[29]

Meanwhile, the overlapped anodic profile in the first 5 cycles of charging at 2.2 and 2.5 V (see the ESI of Fig. S3b†) is related to the oxidation reactions from Li_2S to Li_2S_8. The absence of overpotential in the cathodic profile indicates decreased polarization because the active material migrates to electrochemically stable sites of the TiO_2 nanotubular membrane during the first cycle. The complete upper discharge plateaus suggest that the migrating polysulfides are localized in the cathode region and that severe active material loss has not occurred. The appearance of the vertical voltage rise at 2.8 V typically indicates a complete charge process. The initial discharge capacity of the cell with TiO_2 nanograssy membrane is 1499 mA h g^{-1}, which approaches 90% of the theoretical capacity of sulfur (1675 mA h g^{-1}). In subsequent cycles, the overlapping cathodic and anodic peaks maintained their peak shape and displayed no obvious peak intensity changes and potential shifts, which suggested superior cycling stability and highly reversible redox reactions. This superior cyclability from the charging/discharging profiles is in line with the results of the cyclic voltammetry performance of the TiO_2 nanotubular membrane, as shown in Fig. 4a. The high active material utilization results from enriched polysulfide trapping in the TiO_2 nanotubular membrane towards the cathode side. The cycling performance in Fig. 4c reveals that the cells with TiO_2 nanograssy (TNT) membrane have stable cyclability, a high discharge capacity of 618 mA h g^{-1}, and high coulombic efficiency of > 97% for over 100 cycles compared to the conventional PE separator. In the case of the PE separator, it shows an abrupt performance for up to 40 cycles after that the cell performance sets to zero due to the non-polar nature of MWCNT, which affects the trapping of polysulfides.[8] In the case of TNT membrane, it absorbs polysulfides enormously due to the chemical absorption property of highly porous TNT membrane.[27]

The stable cyclability and the high-capacity retention resulted from the synergistic effects of highly nanoporous double-walled open tubes (DWOT) at the bottom part and the extremely high aspect ratio of TiO_2 nanograssy networks at the top part (a stable cycling performance for a comparison with other TiO_2 membranes, as shown in the ESI of Table S1†). Firstly, the natural nanopore networks are critical for allowing the Li-ion to diffuse into the cathode and absorbing the polysulfides during the charge–discharge process, which reduces the degradation of the active material and shows better performance. Secondly, the nanoporous membrane provides the essential pathways for the electrolyte diffusion to localize the catholyte within the cathode region and allows the polysulfides to be captured into the surrounding nano-framework, forming a favorite contact among the electrolyte, active material, and carbon matrix. Thirdly, the interfacial resistance was greatly suppressed by the double-walled open tubes (DWOT) that resulted in high chemisorption of polysulfide also providing continuous electron pathways to enhance sulfur utilization. The impedance analysis shown in Fig. 4b confirmed that the TiO_2 nanograssy membrane has higher ionic conductive kinetics towards the cathode side (smaller the semi-circle)

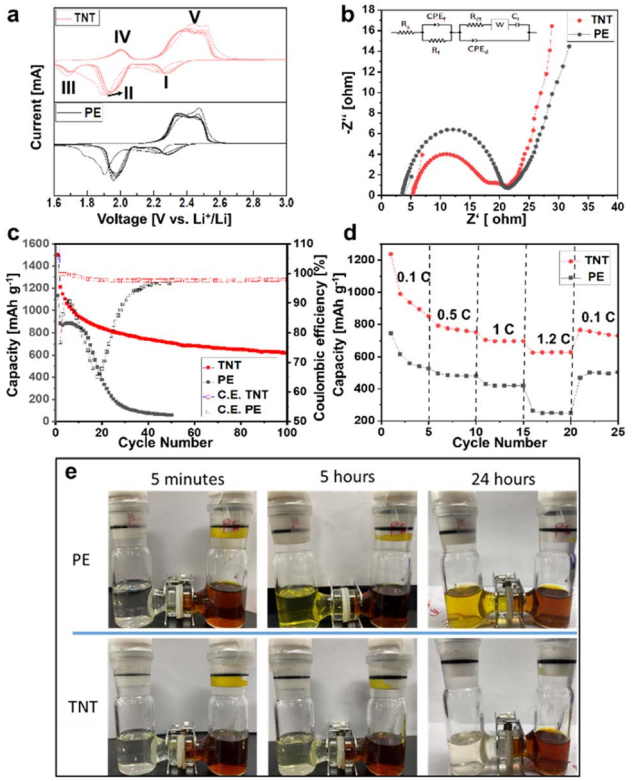

Fig. 4 Electrochemical performance of commercial polyethylene (PE) separator and TiO_2 nanograssy tube (TNT) hybrid membrane in Li–S cells: (a) cyclic voltammetry (CV) *versus* Li/Li + profiles at a scan rate of 0.1 mV s^{-1} over the potential window of 1.6 to 2.8 V for the first 5 cycles, (b) electrochemical impedance spectroscopy (EIS), inset shows the equivalent circuit, (c) cycling performance profiles at 0.1 C-rate, (d) cycling performance profiles at 0.1C to 1.2C of different C-rates, and (e) photographs for the diffusion properties of the Li_2S_x solution through (upper row) polyethylene (PE) separators and (lower row) TiO_2 nanograssy tube (TNT) membrane at different time intervals.

than the commercial polyethylene (PE) separator. Although the TiO_2 nanograssy membrane has a high polysulfides inhibition, it still has the overall semiconducting behavior between the two electrodes with the corresponding value of the charge transfer resistance (R_{ct}) compared to commercial PE separator of approximately 20 Ohm and 21.1 Ohm, respectively. The impedance indicates that the long-range continuity of the TiO_2 nanograssy fiber network facilitates electron transfer and enhances electrochemical kinetics without any carbon-modified membrane in the TiO_2 membrane (see ESI of Table S1†). It is remarkable that the TiO_2 nanograssy (TNT) membrane shows excellent cycling stability under continuously varying C-rates of 0.1C (0.39 mA cm^{-2}), 0.5C (0.69 mA cm^{-2}), 1C (1.7 mA cm^{-2}), 1.2C (4.1 mA cm^{-2}) with loading value of 1.34 mg cm^{-2}. A reversible high and stable capacity of 852.4 mA h g^{-1} was maintained after 5 cycles at a C-rate of 0.1C. At a high C-rate of 0.5C and 1.2C TiO_2 membrane still exhibited the capacity retention of 698 mA h g^{-1} and 624 mA h g^{-1}. It revealed that the fast reaction kinetics notably at the high C-rates are abruptly switched back from 1.2C to 0.1C, and again the capacity recovered to 760.27 mA h g^{-1}. The PE separator showed relatively lower capacity value when switched back into different C-rate values of 0.1C (0.3 mA cm^{-2}),0.5C (0.6 mA cm^{-2}), 1C (1.5 mA cm^{-2}), 1.2C (3.7 mA cm^{-2}) with the loading value of 1.32 mg cm^{-2} due to non-polar nature of the carbon matrix.[8]

Polysulfide dissolution

We investigate the effectiveness of polysulfide absorption with an H-cell configuration. The polysulfides solution of 0.01 M Li_2S_8 in 1,3-dioxalane (DOL) and 1,2-dimethyoxyethane (DME) = 1 : 1 (v: v) was used on the right side of the cell and pure solvent mixture was equilibrated at various time interval as shown in Fig. 4e. The TiO_2 membrane was sandwiched with the same PE separator between the two cells. Double-walled open tubes (bottom part of the membrane) were placed towards the right side of polysulfides solution. After 24 hours of dwell time, the pristine PE separator permeably changed its color to reddish-brown owing to the diffusion of polysulfides. During that time, the contrast of TiO_2 nanograssy (TNT) membrane showed no appreciable color change due to the successive suppression of polysulfides. This can be attributed to the synergistic contribution of the primary physical capture *via* the nanoporous nature in the nanograssy membrane and, moreover, the TiO_2 crystallites on the outer shell of DWOT also contributed to the physical absorption of the Li_2S_x. Based on the chemical interaction between the discharged polysulfides of Li_2S_x and the TiO_2 nanotubular membrane (TNT), it showed enhanced performance in absorbing the large amount of Li_2S_x from the sulfur cathode.

Experimental

Materials

Ti foils (Nilaco, 99.6%, 0.125 mm thickness) were pre-cleaned using ethanol in a sonication bath and dried at room temperature. Anodization was carried out in a two-electrode cell: a degreased Ti foil with a diameter of Ø 19 mm was cut into pieces and welded with the Ti metal current connector for electrical connection as a working electrode and platinum mesh is used as a counter electrode in a high-voltage potentiostat (ODA, OPS-22101, Incheon, Korea) by applying a ramped voltage of 60 V at 1 V s^{-1} for 4 hours in an organic electrolyte of ethylene glycol + 0.5 wt% NH_4F + 1 vol% H_2O.[25,31] After anodization, the sample was rinsed and soaked in ethanol for 10 minutes then finally dried at room temperature. To convert the 'as-prepared' layer into anatase TiO_2; the sample was annealed at 450 °C in the air for 1 hour at a heating rate of 15 °C min^{-1} using a rapid thermal annealer.

Membrane preparation

For the hybridization of the TiO_2 layer, styrene-butadiene rubber (JSR Corporation, SBR 48%) binder was spin-coated at (2000 rpm, 300 seconds) and dried in an oven at 50 °C. In order to form a sacrificial layer, the polymer-coated sample was secondly anodized at 60 V for 20 minutes in the same electrolyte. To obtain the free-standing hybrid membrane, the sample was etched in H_2O_2 (Duksan chemicals, 30 wt%) for 10 minutes at room temperature. After the etching step, the free-standing membrane was rinsed in ethanol and dried at 50 °C for 1 hour.

Morphological characterization

Morphological characterization of the samples was performed using a field-emission scanning electron microscopy Hitachi S4800. The cross-sectional images were taken from the scissors-cut of membrane. X-ray diffraction analysis (XRD) was performed on an X-ray diffractometer (Philips X'pert-MPD) with a Panalytical X'celerator detector with graphite monochromized Cu Kα radiation (λ = 1.54056 Å).

Electrochemical analysis

Coin cell assembly was performed in a dry room to evaluate the performance of the samples. Sulfur powder (Sigma-Aldrich, < 99%, USA) was mixed along with multi-walled carbon nanotubes (MWCNTs, diameter = 9.5 nm, Nanocyl, Belgium) (S : MWCNT = 7 : 3 wt%) in ethanol by a ball-milling process (450 rpm, 30 minutes, 5 cycles). Ethanol was eliminated by the vacuum filtration technique. The obtained MWCNT@S composite cathode material was treated at 70 °C for 24 hours in a vacuum oven to remove any traces of the solvents and then heat treated at 155 °C for 2 hours to diffuse elemental S into the MWCNT network.[43] The MWCNT-based S cathode was obtained with a controlled film thickness of 200 μm on an Al current collector with a mass loading of 1.23 mg cm^{-2} containing the active material: conducting agent: a binder of 70 : 20 : 10 with S/MWCNT : Super-P : Poly (ethylene oxide), which served as a cathode. TiO_2 nanograssy hybrid membrane (25 μm) as a supporting film was attached to the separator facing the nanograssy surface to the cathode part. A 500 μm thick Li-metal foil was used as an anode. The electrolyte was 1 M lithium bis (trifluoromethylsulfonyl) imide (LiTFSI) (Sigma-Aldrich, 99.0%) dissolved in DOL and DME = 1 : 1 (v: v) with a 1 wt% $LiNO_3$ (Sigma-Aldrich, 99.99%) additive as an electrolyte. The coin cell was galvanostatically charged/discharged at a C-rate of 0.1C.

Rate performances with a multichannel battery tester (MACCORE) were evaluated for different C-rates from 0.1C to 1.2C, at a potential range of 1.8–2.8 V. Cyclic voltammetry (CV) and electrochemical impedance spectroscopy (EIS) were conducted on an electrochemical setup (Bio Logic model, VMP3, France). CV was performed at a scan rate of 1 mV s^{-1} in a voltage range of 1.6–3.0 V while EIS was performed after 100 cycles at different bias potentials in a frequency range of 10 kHz to 100 MHz with an AC signal amplitude of 10 mV.[43] The dissolution of Li_2S_8 of (0.01 M) in 1,3-dioxalane (DOL) and 1,2-dimethoxyethane (DME) was studied by comparing the PE separator (W-Scope, pore volume: 43%, pore size: 60 nm, thickness: 16 μm, Tokyo, Japan) and the TiO_2 nanotubular grassy (TNT) membrane as a polysulfides inhibitor in H-cell configuration.

Conclusions

In summary, we have shown the preparation of a free-standing TiO_2 nanotubular hybrid membrane by two-step electrochemical anodization incorporated with polymer hybridization. The TiO_2 nanotubular membrane has bundles of nanograss on the tube top and double-walled nanostructures in the tube. The double-walled nanotubes consist of a porous TiO_2 nanoparticulate inner shell and pure TiO_2 in the outer shell. The nanopores and macroscopic networks of nanograssy tubular layer, which could absorb the soluble polysulfides and channel the electrolyte have the potential to substitute the conventional TiO_2 nanoparticle membrane. Even though a feasibility study on the anodically obtained membrane for Li–S battery was addressed here, there is still room for reinforcing the performance of this novel free-standing TiO_2 nanograssy tubular hybrid membrane in energy storage by further modification with some metal nanoparticles or some conductive materials.

Author contributions

Conceptualization: S. Dasarathan, J. Sung, D. Kim, J.-W. Park. Data curation: Y.-S. Jo, J.-W. Hong. Formal analysis: B.-G. Kim. Funding acquisition: Y.-J. Lee, H.-Y. Choi. Investigation: H.-Y. Choi. Methodology: S. Dasarathan, J. Sung, D. Kim. Project administration: Y.-J. Lee. Resources: J.-W. Park, D. Kim. Software: J. Sung, J.W. Hong. Supervision: B.-G. Kim, D. Kim. Validation: B.-G. Kim, J.-W. Park. Visualization: H.-Y. Choi, Y.-J. Lee. Writing – original draft: S. Dasarathan, D. Kim. Writing – review and editing: D. Kim, J.-W. Park.

Conflicts of interest

"There are no conflicts to declare".

Acknowledgements

This work was supported by the Primary Research Program (23A01030) of the Korea Electro-Technology Research Institute and by the Technology Innovation Program (20014581) of the Ministry of Trade, Industry, and Energy (MOTIE, Korea).

Notes and references

1 C. Xu, B. Xu, Y. Gu, Z. Xiong, J. Sun and X. S. Zhao, Graphene-based electrodes for electrochemical energy storage, *Energy Environ. Sci.*, 2013, **6**, 1388.
2 Y. X. Yin, S. Xin, Y. G. Guo and L. J. Wan, Lithium–Sulfur Batteries: Electrochemistry, Materials, and Prospects, *Angew. Chem., Int. Ed.*, 2013, **52**, 13186.
3 X. W. Zhang, A. Wang, Y. Wang, K. Huang, Z. Yuan, J. Yu, Y. Qiu and J. Yang, Improved cycle stability and high security of Li-B alloy anode for lithium–sulfur battery, *J. Mater. Chem. A*, 2014, **2**, 11660.
4 W. Si, I. Mönch, C. Yan, J. Deng, S. Li, G. Lin, L. Han, Y. Mei and O. G. Schmidt, A Single Rolled-Up Si Tube Battery for the Study of Electrochemical Kinetics, Electrical Conductivity, and Structural Integrity, *Adv. Mater.*, 2014, **26**, 7973.
5 Y. Zhou, C. D. Gu, J. P. Zhou, L. J. Cheng, W. L. Liu, Y. Q. Qiao, X. L. Wang and J. P. Tu, Effect of carbon coating on low temperature electrochemical performance of LiFePO4/C by using polystyrene sphere as carbon source, *Electrochim. Acta*, 2011, **56**, 5054.
6 Z. Lin and C. Liang, Lithium–sulfur batteries: from liquid to solid cells, *J. Mater. Chem. A*, 2015, **3**, 936.
7 A. Manthiram, Y. Fu and Y. Su, Challenges and Prospects of Lithium–Sulfur Batteries, *Acc. Chem. Res.*, 2013, **46**, 1125–1134.
8 Q. Pang, D. Kundu, M. Cuisinier and L. F. Nazar, Surface-enhanced redox chemistry of polysulphides on a metallic and polar host for lithium-sulphur batteries, *Nat. Commun.*, 2014, **5**, 3.
9 Z. Liang, G. Zheng, W. Li, Z. W. Seh, H. Yao, K. Yan, D. Kong and Y. Cui, Sulfur Cathodes with Hydrogen Reduced Titanium Dioxide Inverse Opal Structure, *ACS Nano*, 2014, **8**, 5249.
10 X. Cui, Z. Shan, L. Cui and J. Tian, Enhanced electrochemical performance of sulfur/carbon nanocomposite material prepared *via* chemical deposition with a vacuum soaking step, *Electrochim. Acta*, 2013, **105**, 23.
11 Z. Zhang, Z. Li, F. Hao, X. Wang, Q. Li, Y. Qi, R. Fan and L. Yin, 3D Interconnected Porous Carbon Aerogels as Sulfur Immobilizers for Sulfur Impregnation for Lithium-Sulfur Batteries with High Rate Capability and Cycling Stability, *Adv. Funct. Mater.*, 2014, **24**, 2500.
12 Z. Wang, Y. Dong, H. Li, Z. Zhao, H. Bin Wu, C. Hao, S. Liu, J. Qiu and X. W. D. Lou, Enhancing lithium–sulphur battery performance by strongly binding the discharge products on amino-functionalized reduced graphene oxide, *Nat. Commun.*, 2014, **5**, 5002.
13 Y. Cui, A. Abouimrane, C. J. Sun, Y. Ren and K. Amine, Li–Se battery: absence of lithium polyselenides in carbonate-based electrolyte, *Chem. Commun.*, 2014, **50**, 5576.
14 J. H. Kim, K. Fu, J. Choi, S. Sun, J. Kim, L. Hu and U. Paik, Hydroxylated carbon nanotube enhanced sulfur cathodes for improved electrochemical performance of lithium–sulfur batteriesChem, *Commun*, 2015, **51**, 13682.

15 C. Zhang, H. Bin Wu, C. Yuan, Z. Guo and X. W. Lou, Confining Sulfur in Double-Shelled Hollow Carbon Spheres for Lithium–Sulfur Batteries, *Angew. Chem., Int. Ed.*, 2012, **51**, 9592.

16 W. Zhou, Y. Yu, H. Chen, F. J. Disalvo and H. D., Abruna, Amylopectin Wrapped Graphene Oxide/Sulfur for Improved Cyclability of Lithium–Sulfur Battery, *ACS Nano*, 2013, **7**(10), 8801–8808.

17 H. Wang, Y. Yang, Y. Liang, J. T. Robinson, Y. Li and A. Jackson, Graphene-Wrapped Sulfur Particles as a Rechargeable Lithium–Sulfur Battery Cathode Material with High Capacity and Cycling Stability, *Nano Lett.*, 2011, **11**, 2644.

18 Y. Yang, G. Zheng and Y. Cui, Nanostructured sulfur cathodes, *Chem. Soc. Rev.*, 2013, **42**, 3018.

19 X. Zhou, J. Xie, J. Yang, Y. Zou, J. Tang, S. Wang, L. Ma and Q. Liao, Improving the performance of lithium–sulfur batteries by graphene coating, *J. Power Sources*, 2013, **243**, 993.

20 F. Sun, J. Wang, H. Chen, W. Li, W. Qiao, D. Long and L. Ling, High Efficiency Immobilization of Sulfur on Nitrogen-Enriched Mesoporous Carbons for Li–S Batteries, *ACS Appl. Mater. Interfaces*, 2013, **5**, 5630.

21 Y. Yao, H. Liu, G. Li, H. Peng and K. Chen, Synthesis and electrochemical performance of phosphate-coated porous LiNi1/3Co1/3Mn1/3O2 cathode material for lithium-ion batteries, *Electrochim. Acta*, 2013, **113**, 340.

22 J. Rong, M. Ge, X. Fang and C. Zhou, Solution Ionic Strength Engineering As a Generic Strategy to Coat Graphene Oxide (GO) on Various Functional Particles and Its Application in High-Performance Lithium–Sulfur (Li–S) Batteries, *Nano Lett.*, 2014, **14**, 473.

23 S. Lu, Y. Chen, X. Wu, Z. Wang and Y. Li, Experimental visualization of the diffusion pathway of sodium ions in the $Na_3[Ti_2P_2O_1F]$ anode for sodium-ion battery, *Sci. Rep.*, 2014, **4**, 4.

24 X. Ji, S. Evers, R. Black and L. F. Nazar, Stabilizing lithium–sulphur cathodes using polysulphide reservoirs, *Nat. Commun.*, 2011, **2**, 325.

25 S. Pervez, D. Kim, C. H. Doh, U. Farooq, A. Yaqub, J. H. Choi, Y. J. Lee and M. Saleem, High areal capacity for battery anode using rapidly growing self-ordered TiO_2 nanotubes with a high aspect ratio, *Mater. Lett.*, 2014, **137**, 347.

26 W. Zhou, X. Xiao, M. Cai and L. Yang, Polydopamine-Coated, Nitrogen-Doped, Hollow Carbon–Sulfur Double-Layered Core–Shell Structure for Improving Lithium–Sulfur Batteries, *Nano Lett.*, 2014, **14**, 5250.

27 Z. W. Seh, W. Li, J. J. Cha, G. Zheng, Y. Yang, M. T. McDowell, P. C. Hsu and Y. Cui, Sulphur–TiO_2 yolk–shell nanoarchitecture with internal void space for long-cycle lithium–sulphur batteries, *Nat. Commun.*, 2013, **4**, 1331.

28 X. Tao, J. Wang, Z. Ying, Q. Cai, G. Zheng, Y. Gan, H. Huang, Y. Xia, C. Liang, W. Zhang and Y. Cui, Strong Sulfur Binding with Conducting Magnéli-Phase TinO2n–1 Nanomaterials for Improving Lithium–Sulfur Batteries, *Nano Lett.*, 2014, **14**, 5288.

29 A. Sabbaghi, C. H. Wong, X. Hu and F. L. Y. Lam, Titanium dioxide nanotube arrays (TNTAs) as an effective electrocatalyst interlayer for sustainable high-energy density lithium-sulfur batteries, *J. Alloys Compd.*, 2022, **899**, 163268.

30 Y. Chen, W. Tang, J. Ma, B. Ge, X. Wang, Y. Wang, P. Ren and R. Liu, Nickel-decorated TiO_2 nanotube arrays as a self-supporting cathode for lithium-sulfur batteries, *Front. Mater. Sci.*, 2020, **14**, 266–274.

31 S. Dasarathan, M. Ali, T. J. Jung, J. Sung, Y. C. Ha, J. W. Park and D. Kim, Vertically Aligned Binder-Free TiO_2 Nanotube Arrays Doped with Fe, S and Fe-S for Li-ion Batteries, *Nanomaterials*, 2021, **11**, 1.

32 J. K. Ha, Y. G. Gwag, J. S. Song, G. B. Cho, H. J. Ahn, J. H. Ahn and K. K. Cho, Effect of surface coating on the electrochemical performance of cathode made of sulfur–loaded TiO_2 nanotube arrays, *J. Alloys Compd.*, 2018, **737**, 248.

33 Z. J. Zhang, J. Zhao, Z. J. Qiao, J. M. Wang, S. H. Sun, W. X. Fu, X. Y. Zhang, Z. Y. Yu, Y. H. Dou, J. L. Kang, D. Yuan, Y. Z. Feng and J. M. Ma, Nonsolvent-induced phase separation-derived TiO_2 nanotube arrays/porous Ti electrode as high-energy-density anode for lithium-ion batteries, *Rare Met.*, 2021, **40**, 393.

34 Y. Zhao, W. Zhu, G. Z. Chen and E. J. Cairns, Polypyrrole/TiO2 nanotube arrays with coaxial heterogeneous structure as sulfur hosts for lithium sulfur batteries, *J. Power Sources*, 2016, **327**, 447.

35 M. Zhang, C. Wang, H. Li, J. Wang, M. Li and X. Chen, Enhanced performance of lithium ion batteries from self-doped TiO_2 nanotube anodes *via* an adjustable electrochemical process, *Electrochim. Acta*, 2019, **326**, 134972.

36 D. Kim, A. Ghicov and P. Schmuki, TiO_2 Nanotube arrays: Elimination of disordered top layers ("nanograss") for improved photoconversion efficiency in dye-sensitized solar cells, *Electrochem. Commun.*, 2008, **10**, 1835.

37 S. P. Albu, A. Ghicov, J. M. Macak, R. Hahn and P. Schmuki, Self-Organized, Free-Standing TiO_2 Nanotube Membrane for Flow-through Photocatalytic Applications, *Nano Lett.*, 2007, **7**, 1286.

38 S. P. Albu, A. Ghicov, S. Aldabergenova, P. Drechsel, D. LeClere, G. E. Thompson, J. M. Macak and P. Schmuki, Formation of Double-Walled TiO2 Nanotubes and Robust Anatase Membranes, *Adv. Mater.*, 2008, **20**, 4135.

39 S. So, I. Hwang, F. Riboni, J. Yoo and P. Schmuki, Robust free-standing flow-through TiO_2 nanotube membranes of pure anatase, *Electrochem. Commun.*, 2016, 73–78.

40 G. F. Ortiz, l. Hanzu, T. Djenizian, P. Lavelo, J. L. Tirado and P. Knauth, Alternative Li-Ion Battery Electrode Based on Self-Organized Titania Nanotubes, *Chem. Mater.*, 2009, **21**(1), 63–67.

41 G. D. Salian, M. Krbal, H. Sopha, C. Lebouin, M.-V. Coulet, J. Michalicka, L. Hromadko, A. T. Tesfayer, J. M. Macak and T. Djenizian, Self-supported sulphurized TiO_2 nanotube layers as positive electrodes for lithium microbatteries, *Appl. Mater. Today*, 2019, 257–264.

42 P. Roy, S. Berger and P. Schmuki, TiO_2 Nanotubes: Synthesis and Applications, *Angew. Chem., Int. Ed.*, 2011, **50**, 2904–2939.

43 S.-C. Jo, J.-W. Hong, I.-K. Choi, M.-J. Kim, B.-G. Kim, Y.-J. Lee, H.-Y. Choi, D. Kim, T.-Y. Kim, K.-J. Baeg and J.-W. Park, Multimodal Capturing of Polysulfides by Phosphorus-Doped Carbon Composites for Flexible High-Energy-Density Lithium–Sulfur Batteries, *Small*, 2022, **18**(21), 2200326.

44 B. Chen, J. Sha, W. Li, F. He, E. Liu, C. Shi, C. He, J. Li and N. Zhao, Graphene Oxide-Assisted Synthesis of Micro sized Ultrathin Single-Crystalline Anatase TiO_2 Nanosheets and Their Application in Dye-Sensitized Solar Cells, *ACS Appl. Mater. Interfaces*, 2016, **8**(4), 2495–2504.

45 B. Chen, Y. Meng, F. Xie, F. He, C. He, K. Davey and N. Zhao, 1D Sub-Nanotubes with Anatase/Bronze TiO_2 Nanocrystal Wall for High-Rate and Long-Life Sodium-Ion Batteries, *Adv.Mater.*, 2018, **30**, 1804116.